Extensive transcriptional complexity during hypoxia-regulated expression of the myoglobin gene in cancer

Bicker, Anne ; Dietrich, Dimo ; Gleixner, Eva ; Kristiansen, Glen ; Gorr, Thomas A ; Hankeln, Thomas

Abstract: Recently, the ectopic expression of myoglobin (MB) was reported in human epithelial cancer cell lines and breast tumor tissues, where MB expression increased with hypoxia. The better prognosis of MB-positive breast cancer patients suggested that the globin exerts a tumor-suppressive role, possibly by impairing mitochondrial activity in hypoxic breast carcinoma cells. To better understand MB gene regulation in cancer, we systematically investigated the architecture of the human MB gene, its transcripts and promoters. In silico analysis of transcriptome data from normal human tissues and cancer cell lines, followed by RACE-PCR verification, revealed seven novel exons in the MB gene region, most of which are untranslated exons located 5'-upstream of the coding DNA sequence (CDS). Sixteen novel alternatively spliced MB transcripts were detected, most of which predominantly occur in tumor tissue or cell lines. Quantitative RT-PCR analyses of MB expression in surgical breast cancer specimen confirmed the preferential usage of a hitherto unknown, tumor-associated MB promoter, which was functionally validated by luciferase reporter gene assays. In line with clinical observations of MB up-regulation in avascular breast tumors, the novel cancer-associated MB splice variants exhibited increased expression in tumor cells subjected to experimental hypoxia. The novel gene regulatory mechanisms unveiled in this study support the idea of a non-canonical role of MB during carcinogenesis.

DOI: https://doi.org/10.1093/hmg/ddt438

HMG Advance Access published October 1, 2013

Human Molecular Genetics, 2013 **1–12**
doi:10.1093/hmg/ddt438

Extensive transcriptional complexity during hypoxia-regulated expression of the myoglobin gene in cancer

Anne Bicker[1], Dimo Dietrich[2], Eva Gleixner[1,†], Glen Kristiansen[2], Thomas A. Gorr[3,4] and Thomas Hankeln[1,*]

[1]Institute of Molecular Genetics, Johannes Gutenberg University, J.J. Becherweg 30a, Mainz 55099, Germany, [2]Institute of Pathology, University Hospital Bonn, Sigmund-Freud-Str. 25, Bonn 53127, Germany, [3]Center for Pediatrics and Adolescent Medicine, Clinic IV, Division of Pediatric Hematology and Oncology, University Medical Center Freiburg, Mathildenstrasse 1, Freiburg 79106, Germany and [4]Institute of Veterinary Physiology, Vetsuisse Faculty, University of Zurich, Winterthurerstrasse 260, Zurich 8057, Switzerland

Received July 11, 2013; Revised and Accepted September 4, 2013

Recently, the ectopic expression of myoglobin (MB) was reported in human epithelial cancer cell lines and breast tumor tissues, where MB expression increased with hypoxia. The better prognosis of MB-positive breast cancer patients suggested that the globin exerts a tumor-suppressive role, possibly by impairing mitochondrial activity in hypoxic breast carcinoma cells. To better understand *MB* gene regulation in cancer, we systematically investigated the architecture of the human *MB* gene, its transcripts and promoters. *In silico* analysis of transcriptome data from normal human tissues and cancer cell lines, followed by RACE-PCR verification, revealed seven novel exons in the *MB* gene region, most of which are untranslated exons located 5′-upstream of the coding DNA sequence (CDS). Sixteen novel alternatively spliced *MB* transcripts were detected, most of which predominantly occur in tumor tissue or cell lines. Quantitative RT–PCR analyses of *MB* expression in surgical breast cancer specimen confirmed the preferential usage of a hitherto unknown, tumor-associated *MB* promoter, which was functionally validated by luciferase reporter gene assays. In line with clinical observations of MB up-regulation in avascular breast tumors, the novel cancer-associated *MB* splice variants exhibited increased expression in tumor cells subjected to experimental hypoxia. The novel gene regulatory mechanisms unveiled in this study support the idea of a non-canonical role of MB during carcinogenesis.

INTRODUCTION

Myoglobin (MB) was the first oxygen-binding respiratory protein described to appear in extravascular locations (1,2). It is mainly expressed in skeletal and cardiac muscle of vertebrates at high micro- or millimolar concentrations (3–5). Owing to its high O_2-binding affinity (P_{50} ~1 Torr), MB supports the intracellular diffusion of O_2 from the sarcolemma to the mitochondria (6,5). In addition, MB functions in short-term O_2 storage in contracting muscles for a steadier O_2 supply to the mitochondria (4). Upon cellular hypoxia, MB has been described to decrease the level of reactive oxidative stress and to detoxify harmful excess nitric oxide ($NO^{\bullet}$) and nitrite (7–10).

MB expression was further reported in various human malignant tumors and tumor cell lines that did not originate from myocytic precursors, including acute leukemia, desmoplastic small round cell tumors, breast carcinoma, colon carcinoma and non-small cell lung cancer (11–15). In example, 40% of invasive breast carcinomas were found to exhibit pronounced MB expression (14). Comparing *MB* levels in breast tumor biopsies and healthy ductal tissue counterparts from the same individuals revealed on average a 350-fold higher abundance of *MB* transcripts in the cancer tissues (14). In a corresponding Kaplan–Meier analysis, the overall survival of 917 primary breast cancer cases was monitored and correlated to their MB and estrogen receptor

*To whom correspondence should be addressed at: Institute of Molecular Genetics, Johannes Gutenberg University, J.J. Becherweg 30a, Mainz 55099, Germany. Tel: +49 61313923277; Fax: +49 61313924585; Email: hankeln@uni-mainz.de
†Present address: Center for Systems Biology, University of Freiburg, Freiburg 79104, Germany.

alpha (ERα) status. Despite the fact that patients with ERα-positive tumors generally have a better outcome, and that mammary carcinomas displayed a tight association between the presence of MB and ERα, we also documented the favorable prognosis of ERα-deficient breast tumors with high MB content (ER-/MB+) relative to ERα-deficient/MB-deficient (ER-/MB-) entities (14). Thus, MB is of prognostic value and might confer tumor-suppressive activity *in vivo*.

To investigate the possible function of MB in a tumor context, lentiviral gene transfer was employed to overexpress mouse Mb in the MB-null A549 human lung cancer cell line (16). Resulting experimental tumors expressing ectopic Mb displayed reduced hypoxia, minimal levels of the O_2-sensitive alpha subunit of the hypoxia-inducible factor (HIF-1α), lower vessel density along with a more differentiated cancer cell phenotype and largely suppressed metastatic spreading. The authors correlated these beneficial outcomes of Mb overexpression with the reduction of tumor hypoxia (16). However, this approach seems somewhat artificial, since the total amount of Mb in the engineered cancer cells was similar to MB levels in human muscle [i.e. (MB) ∼200–300 μM], while endogenously occurring MB protein levels in breast cancer cells are several hundred-fold lower (14). Therefore, it remains doubtful whether MB in tumors is sufficiently abundant to confer meaningful O_2 supply capacity and to maintain aerobiosis in temporarily hypoxic cancer cells. In line with a negligible role of endogenous MB in O_2 transport in breast tumor cells, high-resolution respirometry on stable *MB* knockdown clones of suspended MDA-MB468 breast cancer cells revealed, when compared with *MB* proficient controls, statistically indistinguishable *in vitro* $P_{50}(O_2)$ values (17). Apparently, endogenous MB in breast tumors and breast cancer cells may thus exert a non-classical molecular function. Along this line, it has been proposed that MB may regulate oxidative/nitrosative stress in cancer cells, e.g. by its ability to scavenge toxic $NO^{\bullet}$ under hypoxic conditions (13). Our own experiments using siRNA-driven *MB* silencing in MDA-MB468 breast cancer cells indicated that MB interferes with the capacity of the mitochondria specifically in hypoxic carcinoma cells. MB was additionally found to influence proliferation and motility of these cells, yet in ways not directly related to the facilitated diffusion or storage of O_2 (17).

The attractive hypothesis that MB might have tumor-suppressive properties raised the question for the gene regulatory mechanisms driving the transcription of the globin in cancer cells. MB immunostaining on breast ductal carcinoma *in situ* (DCIS) entities revealed a gradient of MB expression, which correlated with hypoxia markers (17). Several publications also reported the robust increase of *MB* concentrations by transcriptional up-regulation in epithelial cancer cells subjected to hypoxia (13–15). Analogous to the functional discrepancies between carcinoma and myocytic MB, this hypoxia-mediated increase in cancer *MB* expression is also at odds with known regulatory mechanisms of *MB* in muscles. According to the current view, hypoxia acts only as an effective regulatory stimulus of *MB* expression in muscle when it is accompanied by other triggers (such as exercise) (18). This observation is concordant with the fact that the standard muscle *MB* promoter region apparently lacks canonical HIF-binding cis-elements (i.e. hypoxia response elements, HREs) and hypoxia inducibility (19). Recently, however, one alternative *MB* transcript (NM_203377) was reported to originate from a different, non-standard promoter site, which appeared predominantly active in the breast cancer cell line MDA-MB468 (17). This alternative *MB* mRNA was 300-fold increased over the standard transcript in the breast cancer cell line. Moreover, the alternative mRNA was 2.2-fold induced in cells challenged by prolonged hypoxia, compared with normoxic samples. However, it remained unclear whether the novel transcript occurs also in clinical specimen *in vivo* or in other cell lines. In addition, a novel candidate HRE, located 2.8 kb upstream of the translation start site of the *MB* gene was identified, which enhanced reporter gene transcription by ∼43% in hypoxic MDA-MB468 cells. Apparently, this element is therefore only a minor contributor to hypoxic *MB* induction (17).

In the present study, we systematically characterized the spectrum of *MB* transcript variants and their initiation sites by transcriptome sequence data mining and experimental verification. We evaluated the expression levels of novel, alternative *MB* transcripts in various human tissues and cancer cell lines by the quantification of RNA-Seq data. To account for mouse as a model organism, we examined conservation of the human and mouse *Mb* gene structures. Expression rates of *MB* transcript variants were compared in normoxic and hypoxic cultures of a breast and a colon cancer cell line to elucidate how diminished O_2 supply impacts on *MB* gene regulation in different cancer backgrounds. The biological relevance of cancer-associated, hypoxia-inducible *MB* transcripts was then validated in breast cancer biopsies, and the functionality of a novel promoter was studied by dual luciferase reporter assays (DLRAs). To identify functional differences between the cancer-linked *MB* transcript variants, the influence of an alternatively spliced upstream open reading frame (uORF) on globin translation efficiency was examined.

RESULTS

A revised structure of the human *MB* gene

To identify the full spectrum of alternative transcripts from the human *MB* gene, we first mined available *MB* transcriptome data from the NCBI UniGene EST (expressed sequence tag) database (for a list of representative ESTs supporting alternative *MB* transcripts, see Supplementary Material, Table S1). RT–PCR reactions using cDNA from the breast and colon cancer cell lines MDA-MB468 and DLD-1, respectively, were then performed to verify the *in silico*-predicted utilization of *MB* exon sequences (Supplementary Material, Table S2). Amplicons were sequenced to assemble a list of novel exons and splice variants of the human *MB* gene (Supplementary Material, Fig. S1, Fig. 1). EST and RT–PCR data from cancer cells revealed six novel exons located within the 5′UTR (untranslated region) of the human *MB* gene and one alternative non-coding start exon located between the first and the second coding DNA sequence (CDS)-containing exon (Fig. 1). Considering all known and newly annotated exons, the genomic sequence of human *MB* now encompasses 31 796 bp (coordinates in genome build 37/hg19 are q12.3 Chr 22: 36 002 811–36 034 607), thus about doubling the size of the current human *MB* gene annotation in the NCBI database (Supplementary Material, Fig. S1 and Fig. 1). Exons were numbered in 5′ > 3′-direction, tagging untranslated exons with a ‘u’ and exons that encode at least part

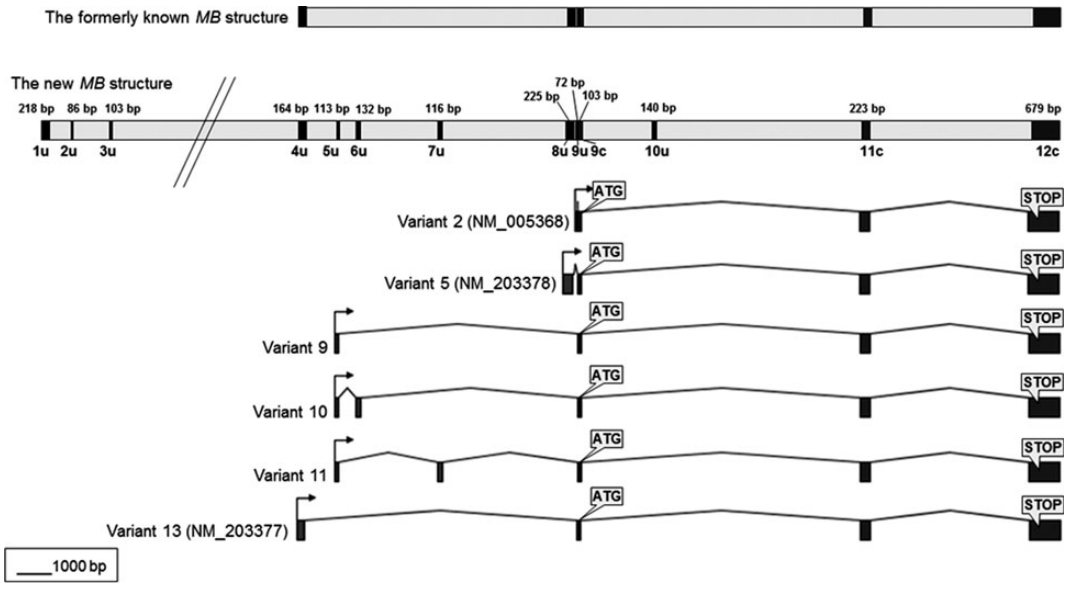

Figure 1. Revised exon-intron structure of the human *MB* gene and its former version (top). Exons are shown as dark boxes with their sizes in bp written on top. Untranslated and CDS-encoding exons are tagged with a 'u' or 'c', respectively. The most prominent protein encoding splice variants from muscle (variants 2 and 5) and from cancer-related samples (variants 9–11, 13) are shown, including the start and stop codons of the *MB*-CDS.

of the CDS, with a 'c'. The three long-known CDS-containing exons 1–3 were thus renamed as exons 9 c, 11 c and 12 c, respectively (20).

From the newly detected exons, we were able to infer 16 novel splice variants in addition to three previously annotated ones (Supplementary Material, Fig. S1). Variant 2 corresponds to the NCBI-annotated transcript NM_005368.2 (AceView transcript b) and the first published *MB* structure (20). Variant 13 equals NM_203377.1 [AceView transcript d; also see (17)] and variant 5 has been annotated as NM_203378.1 (AceView transcript c). According to EST data, these previously annotated transcripts are the most common ones. The CDS-encoding exons 11 c and 12 c were present in all known and novel splice forms, and most variants also contained exon 9 c with the canonical start codon. Thus, 9 out of 19 transcript variants encode the standard MB protein as found in muscle, whereas all others translate into either no or a truncated MB protein. All introns are equipped with consensus splice sites.

The integrity of the novel protein-encoding *MB* transcripts was confirmed via 5′ and 3′RACE, using total RNA from the MDA-MB468 cell line. In the case of transcript variants 9, 10 and 11, the sequences resulting from 5′RACE reactions suggested the first exon (exon 5 u) to start 25 bp upstream of the *MB* transcript version annotated by AceView. The splice variant 13, starting with exon 4 u, was identified to contain an additional 15 bp when compared with the AceView annotation. We further approved the integrity of variant 19, starting at exon 1 u, via 5′ RACE (Supplementary Material, Fig. S1).

Phylogenetic conservation of the *MB* gene

A search for evolutionary conserved regions within the *MB* gene was conducted to reveal stretches of most important biological function. BLASTN pairwise local alignments of human *MB* and the respective gene regions from other species (Supplementary Material, Table S3) showed that exon 9 c displays the highest sequence conservation. This conservation ranged from 100 to 76% identity to *MB* of chimp and chicken, respectively. The other CDS-encoding exons 11 c and 12 c were also highly conserved in mammals and birds with percent identities ranging from 99 to 70%. Regarding the non-coding 5′UTR, the alignments showed a gradual exon conservation between vertebrate species (Supplementary Material, Table S3). Exons located proximal to the CDS of the globin (such as 8 u) tended to show higher conservation than distant exons, suggesting a lower selection pressure on the 5′region of the *MB* gene in evolution.

Owing to the importance of mouse (*Mus musculus*) as the prime mammalian model organism for biomedical research, a comparison of human and mouse *Mb* gene structures (coordinates in mouse genome build 38/mm10 are qD3 Chr15:77 015 487–77 050 668) for synteny was of particular interest. For this, all mouse ESTs available on NCBI Unigene were annotated in terms of exon presence and tissue type. Equivalent to the human *MB* gene, mouse *Mb* exons were renamed numerically in $5' > 3'$ orientation. Two novel upstream exons and four additional splice variants were detected in mouse (Supplementary Material, Fig. S2b). However, conservation among vertebrates turned out to be very limited: all CDS-containing exons and human exon 8 u, equivalent to exon 4 u in mice (Supplementary Material, Fig. S2b) showed the (expected) sequence conservation, whereas all other human and mouse *Mb* upstream non-coding exons were not alignable and are thus not conserved between the two taxa (Supplementary Material, Fig. S2a). A reason might be that ∼56% of the genomic area encompassing the 5′UTR of human *MB* consist of repetitive elements, such as Alu and L1 elements typical for primate genomes (Supplementary Material, Fig. S3).

Tissue-specific expression of *MB* transcript variants

To identify tissue-specific *MB* splicing patterns, all ESTs ($n =$ 972) were assigned to their tissues of origin (Supplementary

Material, Fig. S1). Expectedly, the standard *MB* transcript (variant 2), represented by 557 ESTs, was most prominently seen in skeletal and heart muscle, and to a much lesser extent in smooth muscle tissues. At least 8 of the 16 novel transcripts were also expressed in muscle tissues, but are only represented by very few EST reads ($n = 13$). Fifteen EST entries, corresponding to eight *MB* transcript variants, were observed in data sets from a large variety of non-muscular tissues, including liver, lung, prostate, testis and sciatic nerve (Supplementary Material, Fig. S1). In cancer cell lines, EST analysis ($n = 8$ reads) and RT–PCR experiments demonstrated the presence of 12 out of the 19 *MB* splice variants. As suggested by our previous study (17) and now confirmed by EST data, transcript variant 13 appeared to be one of the major transcripts expressed in cancer cell lines. In addition, three other protein-coding *MB* transcripts were found in the breast and colon cancer cell lines, i.e. variants 9 (AceView transcript a), 10 and 11 (AceView transcript f), which all have a common transcriptional start at exon 5 u (Fig. 1). The MB-coding variant 19 was only detectable in MDA-MB468 cells, but missing in DLD-1 cells.

To infer relative expression profiles of different body tissues and cancer cell lines, we additionally analyzed 41 RNA-Seq data sets from *MB* expressing human tissues and cancer cell lines (Supplementary Material, Table S4). Sequence reads were mapped against the human *MB* CDS-containing exons and the 5′UTR starting exons, quantified and normalized. Transcription of *MB*-CDS encoding exons was on average 25-fold and 333-fold higher in heart muscle than in normal breast and colon tissue, respectively (Fig. 2). We noted that the mRNA expression measured in breast tissues appeared higher than expected from protein studies (14), and might therefore be partly due to contamination with myocytes. In the cancer cell lines, MDA-MB468, MCF-7, LNCaP and DLD-1, average CDS-exon expression was ~115-fold lower than in heart tissue (Fig. 2).

In addition, great differences were noted in the utilization frequency of the alternative 5′UTR starting exons among the investigated data sets. As expected from our EST analyses, starting exons 8 u and 9 u are predominantly used in muscle and heart, whereas upstream exons 4 u and 5 u are distinctly underrepresented in non-cancerous tissues (Fig. 2). For instance, in human heart those transcripts starting at exon 9 u are ~800 times more abundant than those starting with exon 5 u (Fig. 2). In contrast, cancer cell lines such as MB468, DLD-1 and LNCaP as well as prostate tumor biopsies only express *MB* transcripts starting at upstream exons 4 u and 5 u, yielding mRNA variants 9, 10, 11 and 13 (Supplementary Material, Fig. S1). Since there were no reads mapping to the start exons 1 u, 2 u and 10 u in all analyzed transcriptomes, we do not expect their associated *MB* transcripts to typically appear in cancer cells.

Quantification of *MB* transcript variants in cancer cell lines

In silico analyses of RNA-Seq data sets (Supplementary Material, Table S4) and analyses of cDNAs from MDA-MB468 and DLD-1 cells using exon junction-spanning primers to specifically distinguish between splice variants revealed that the protein-coding *MB* mRNA variants 9, 10, 11 and 13 are present in cancer cell lines. Therefore, these mRNAs might be crucial for the expression of functional MB in tumor tissues. Based on this idea, we quantified the expression of these *MB* transcripts in MDA-MB468 cells and in DLD-1 cells via quantitative real-time reverse-transcriptase PCR (qRT–PCR). Compared with the standard muscle transcript (variant 2), normoxic MDA-MB468 cells produced 374–708-fold higher quantities of the alternative *MB* transcript variants 9, 10 and 11 (Fig. 3). Even transcript variant 13 is significantly more strongly expressed than variant 2 in the breast cancer cell line, although it accounts for only 2% of all transcripts in MDA-MB468 cells. Since the amount of splice variants 9, 10 and 11 greatly exceeded that of variant 2 also in the colon cancer cell line DLD-1, these mRNAs appear to dominate the transcriptional profile of *MB* in a more widespread fashion in epithelial cancer cells.

Hypoxia induction of *MB* transcripts in cancer cell lines

Our previous work pointed to tissue hypoxia as a contributing stimulus of MB expression in DCIS entities (17). We also noted that transcripts corresponding to the cancer-associated *MB* splice variant 13 (starting with exon 4 u) were 2.2-fold up-regulated in MDA-MB468 cells subjected to 1% O_2 for 72 h (17). Equivalent to those experiments, we now compared the abundance of novel, protein-coding cancer-associated *MB* splice forms among the cDNA samples of MDA-MB468 cells and DLD-1 cells raised under hypoxic (72 h, 1% O_2) and normoxic (72 h, air) conditions via qRT–PCR. Relative to normoxic oxygen supply, transcripts variants 9, 10 and 11 showed a statistically significant 3- to 3.5-fold increase in MDA-MB468 and a 1.5- to 2.1-fold up-regulated expression in DLD-1 cells in response to oxygen deprivation (Fig. 3). As a result, splice variants 9, 10 and 11 (all transcribed from exon 5 u) most likely underlie the hypoxia-mediated increase of *MB* in breast and colon cancer cell lines [see (17) for western blot evidence].

Detection of *MB* transcript variants in breast cancer tissues

To prove the relevance of alternative *MB* transcripts in clinically relevant human breast cancer specimens, we also investigated biopsies of 21 breast cancer patients. Following surgical resection of the tumors, tissue specimens were first tested for MB positivity by immunostaining. After RNA extraction and cDNA synthesis, the four protein-encoding *MB* splice forms most commonly found in cancer cell lines and the standard transcript variant 2 were quantified by qRT–PCRs in each tumor sample. In line with our *in vitro* data of breast and colon cancer cell lines, the *MB* transcripts 9, 10 and 11 also represented the dominant *MB* mRNA fraction in the breast cancer cases (Fig. 4A). Compared with the sum of variants 9, 10 and 11, expression of the *MB* standard transcript variant 2 was on average 14-fold suppressed in tumors. The vast majority of the cancer cases expressed variant 9 at maximal quantities, followed by variant 11 and variant 10. In conclusion, the promoter upstream to their common start exon 5 u is the most active driver of *MB* transcription in breast tumors, while the muscle-associated standard promoter most likely plays only a minor role. The *MB* splice variant 13, previously described in the breast cancer cell line MDA-MB468 (17), was weakly expressed in tumor specimens. Compared with the ~26-fold more abundantly present variants 9, 10 and 11 (Fig. 4A), variant 13 is probably of minor importance in an *in vivo* context.

Hypoxia inducibility of *MB* transcripts in breast cancer tissues

We have shown so far that the novel *MB* transcript variants 9, 10 and 11 are inducible in hypoxic cancer cell lines. In addition, variant 13 was earlier reported to be up-regulable in breast cancer cells upon challenge with 1% O_2 (17). To correlate the expression of *MB* transcripts with the degree of hypoxia in tumor tissues, we further quantified mRNA levels of the hypoxia-specific biomarker vascular endothelial growth factor A (*VEGFA*) by qRT–PCR. A significant positive Pearson's correlation between *VEGFA* mRNA increase upon hypoxia stimuli and enhanced expression of the *MB* variants 9, 10, 11 ($P < 0.001$) and variant 13 ($P < 0.001$) under hypoxia was found. In addition, the hypoxia induction of *MB* variant 13 correlated strongly and positively with the hypoxia response of the variants 9, 10 and 11 (Pearson, $P < 0.001$). However, no significant correlation was found between the response of *MB* variant 2 to hypoxia and the hypoxia inducibility of *VEGFA* ($P = 0.7$).

In addition, the degree of hypoxic stress was also inferred by performing carbonic anhydrase IX (CAIX) antibody staining in tumor tissue sections adjacent to the ones used for RNA preparation, as the HIF-1α/-2α target gene *CAIX* is a widely used marker of local tissue hypoxia in solid malignancies. Most tumors with strong *MB* transcription were also CAIX positive (Fig. 4B), with few cases showing a discrepant result (i.e. sample D). For a biological interpretation, one should take into account that hypoxia is considered a local phenomenon, where totally different O_2 levels may occur in adjacent tissue sections.

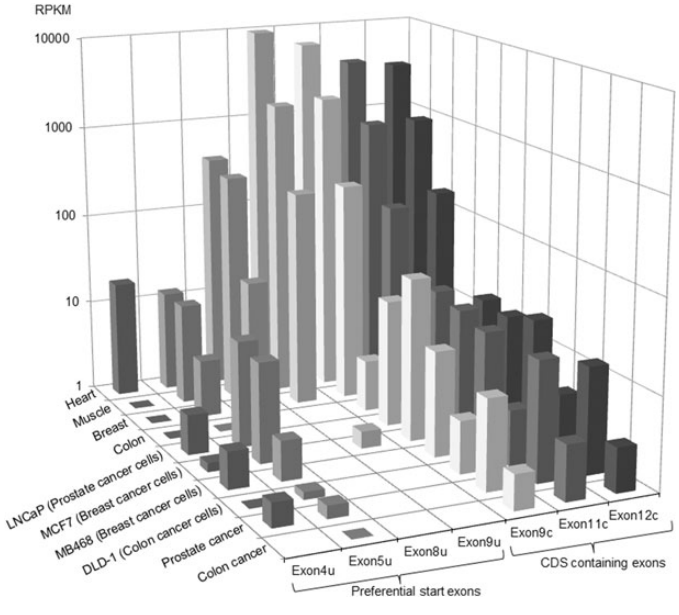

Figure 2. Quantification of *MB* start exon transcription in different human tissues by RNA-Seq read counting. Normalized RPKM values [reads per exon size (in kb) per total reads of the data set (in Mio)] indicate the transcriptional representation of preferential start exon and CDS-containing exons.

Identification of a novel, active *MB* promoter in cancer cells

As described above, in the cancer cell lines MDA-MB 468 and DLD-1 the *MB* mRNA variants 9, 10 and 11 are all transcribed from the same start site, the 5′end of exon 5 u. To characterize the novel gene regulatory region upstream of exon 5 u, we utilized the program Gene2Promoter to identify a 638 bp sequence fragment (Genomatix promotor identification number GXP_2244649; see Fig. 5) as a candidate active promoter sequence. Next, different regions of the predicted promoter sequence were cloned into luciferase reporter vectors to investigate their transcriptional activity in transfected MDA-MB468 cells. The quantified light units of each plasmid were normalized to light intensities of empty vector controls. The largest candidate fragment (692 bp), ranging from 501 bp upstream of the to 191 bp downstream of the transcription start site, was active in breast cancer cells with a 23-fold increase in relative light units (RLUs), when compared with the control (Fig. 5). This fragment fully encompassed the Gene2Promoter-predicted GXP_2244649 sequence. To further characterize transcriptional activities along the promoter region, progressive deletions of the 692 bp region from its 5′ and 3′ends were made and compared in their luciferase readouts to the full-length fragment. Regions containing up to 179 bp upstream to the transcription start site were as active as

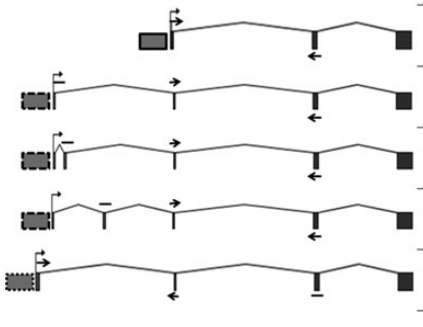

	Total amount at 21% O_2		Fold increase upon 72h, 1% O_2	
	MDA-MB468	DLD-1	MDA-MB468	DLD-1
Var 2	52	71	2.4**	1.5
Var 9	36 665	2 167	3.5***	1.9*
Var 10	19 393	629	3.2*	2.1***
Var 11	27 435	1 151	3.0***	1.5***
Var 13	1 708	98	2.2* (see Ref.(17))	0.9

Figure 3. Expression analysis of *MB* splice variants *in vitro* in normoxic and hypoxic MDA-MB468 breast cancer and DLD-1 colon cancer cells. Numbers in the left half of the table show cDNA copy numbers determined by qRT–PCR, fold-changes in the right half of the table indicate hypoxic up-regulation (*$P < 0.05$; **$P < 0.01$; ***$P < 0.001$; $n = 3$). Primers which are able to distinguish between transcript variants 2, 9–11 and 13, are indicated by arrows above (forward) and underneath (reverse) their respective target exons. The solid, dashed and dotted lines that frame fields of the table indicate promoters common between the splice forms (also shown left to each transcript variant's graph).

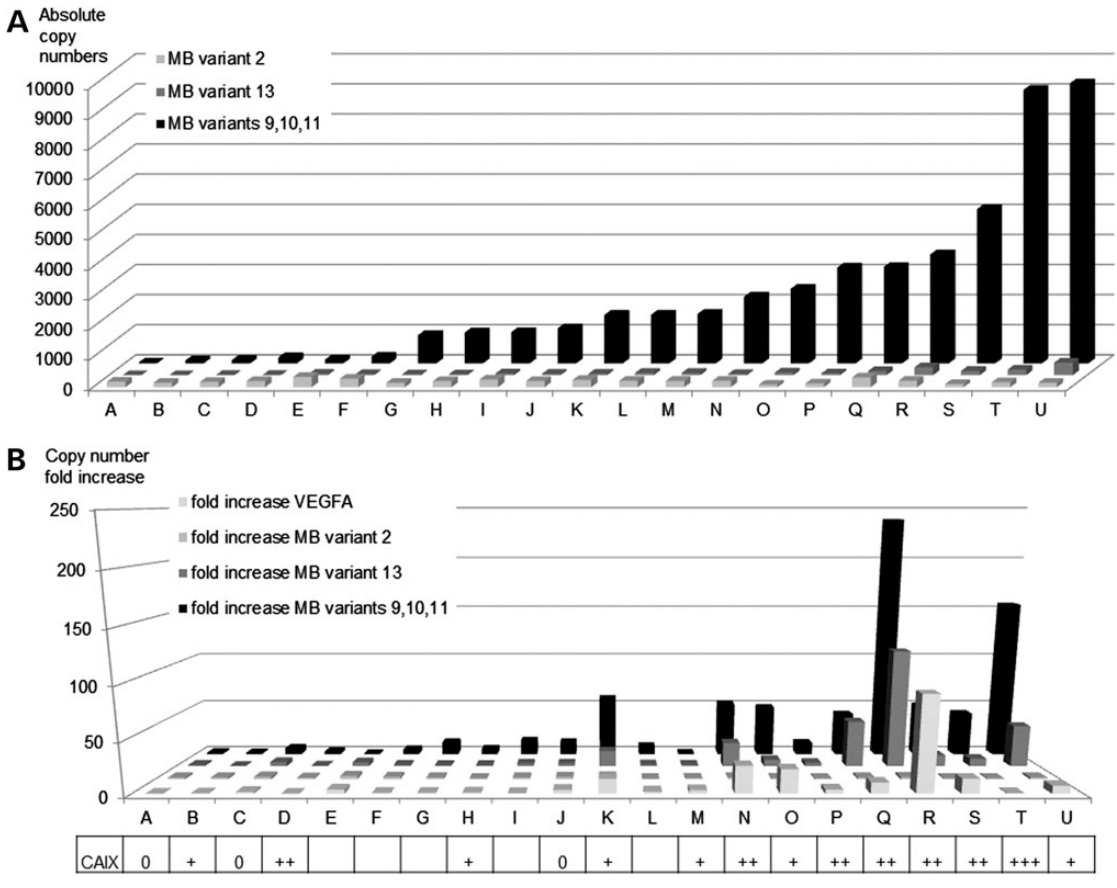

Figure 4. (**A**) Expression analysis of *MB* splice variants in breast cancer biopsies (named A to U). cDNA copy numbers (per 10 ng cDNA) inferred by qRT–PCR are plotted on the *y*-axis (bars). Values for variants 9–11 have been summed up and are shown relative to expression of the minor cancer-associated transcript 13 and the muscle-typic variant 2. (**B**) Correlation between *MB* expression and hypoxia markers in breast tumor specimen. The fold-increase of *MB* variants and *VEGFA* mRNA expression (bars) in tumors versus normal tissue, inferred by qRT–PCR, is shown in relation to the intensity of CAIX immunostaining, as applied to the same tumor sections.

the complete 692 bp fragment in MDA-MB468 cells (i.e. ~50-fold increased reporter gene activity), whereas DNA sections containing only 108 bp upstream of the transcription start site showed much weaker promoter activity (Fig. 5). At the 3′end, DNA sections that ended 25 bp downstream of the transcription start site conferred the strongest reporter gene activation (i.e. ~40-fold increase of RLUs). In contrast, constructs that contained only up to 17 bp downstream of the transcription start site triggered only a 22-fold increase in RLUs (Fig. 5). In result, the most active promoter region upstream of exon 5 u consists of a 204 bp fragment that at least starts 179 bp upstream and ends 25 bp downstream of the transcription start site. A ConSite search for common cis-acting promoter elements revealed a CCAAT-box motif (NF-Y) proximate (57 bp upstream) to the transcription start site (see Fig. 5) that contains a perfectly matching pentanucleotide motif. Owing to its position within the 204 bp fragment, this site might be relevant for promoting the transcription of cancer-associated *MB* mRNAs.

An additional open reading frame within the human *MB* gene

Among the protein-coding *MB* transcripts, variant 11 is unique in containing exon 7 u, which is located on an Alu element. This exon encodes a potential 78 bp uORF, starting at its first basepair. uORFs usually do not encode functional proteins but control the translation efficiency of the following protein coding sequence by facilitating ribosome dissociation (21,22). To test the functionality of the uORF in exon 7 u, pGL3-control reporter assay plasmids were constructed that contain either the full uORF or a point-mutated version (c.-3067A > T, resulting in TTG instead of ATG as a start codon). Neither the uORF, nor its point-mutated version contained a second, additional ATG. To mirror the natural degree of ribosome reinitiation as occurring on the *MB* mRNA variant 11, the exact basepair composition that stretches between the uORF and the *MB*-ORF was added to both plasmids upstream to their luciferase-ATGs. Both constructs were co-transfected with pGL4.74 vectors in MDA-MB468 cells and quantified by DLRAs. Since the unmutated construct containing the uORF (ATG) conferred a 34% decrease in reporter gene translation efficiency relative to the mutated uORF (TTG) construct (Fig. 6), the candidate uORF is indeed able to significantly impair the ribosome attachment upon translation of the *MB* CDS in transcript variant 11.

DISCUSSION

Although MB is traditionally regarded as one of the best-characterized proteins in biochemistry, advances in recent

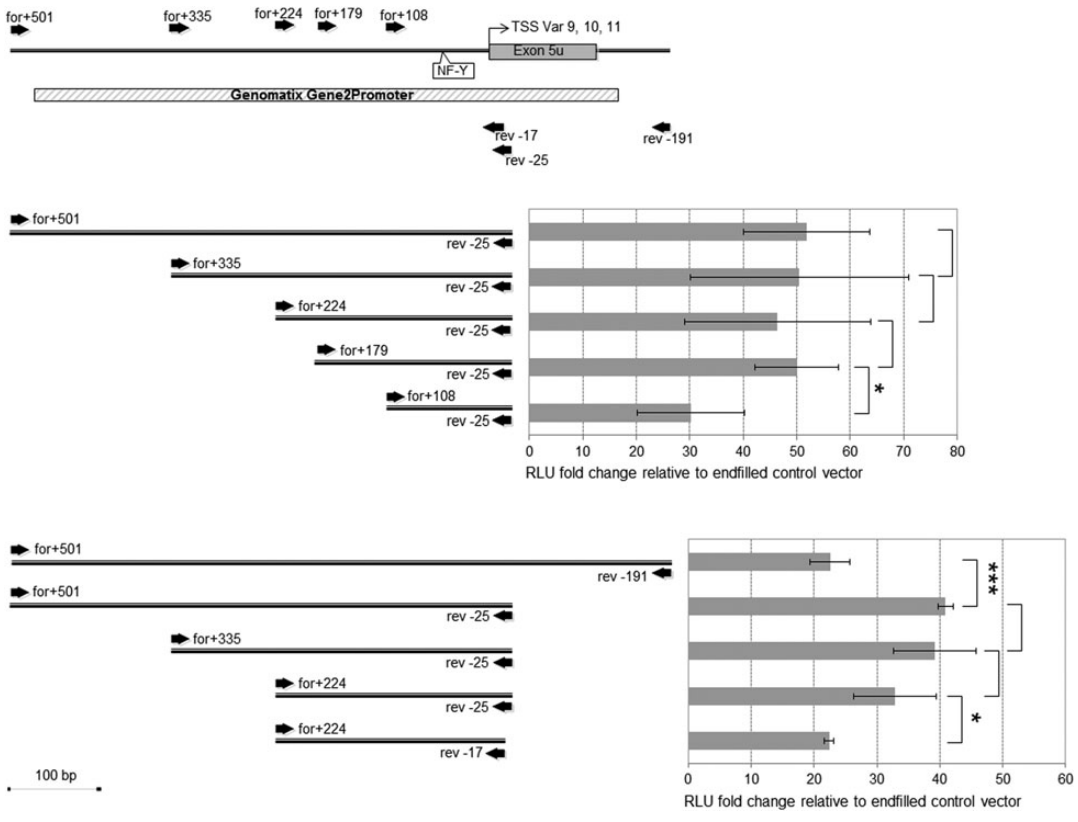

Figure 5. Functional analysis of the promoter section upstream of exon 5 u. DLRAs were conducted on promoter sections that were PCR-amplified from primer sites represented by black arrows. The numbers on the arrows indicate the bp distance to the transcription start site of the *MB* splice variants 9–11. An *in silico*-predicted promoter region and a commonly observed cis-acting promoter element (NF-Y box) are indicated. The average RLUs of each construct were plotted in the bar chart; standard deviations are indicated by error bars ($^{*}P < 0.05$; $^{***}P < 0.001$; $n = 3$).

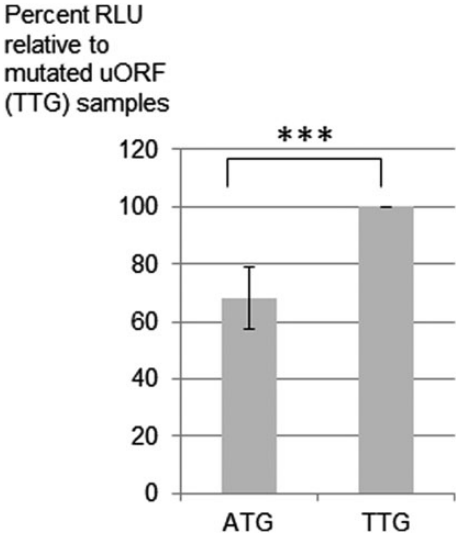

Figure 6. Functional analysis of a uORF in *MB* cassette exon 7 u. DLRA results, plotted as a bar chart, show translational activity of the uORF-containing construct (ATG) and its point-mutated version TTG (c.-3067A > T) for comparison. Standard deviations are indicated by error bars ($^{***}P < 0.001$; $n = 5$).

years have revealed several novel, additional functions of this protein in $NO^{\bullet}$ and ROS (reactive oxygen species) metabolisms, thereby extending its classic role in O_2 supply to muscle cells (5,7,8,23). In parallel, it was shown that beyond its primary localization in cardiac myocytes, skeletal and smooth muscle (3–5,24), MB is expressed at several 'ectopic' sites. Importantly, these additional expression sites include breast cancer, non-small cell lung cancer, colon and ovary carcinomas, desmoplastic small round cell tumors and leukemic bone marrow, as well as derived breast, colon and osteosarcoma cancer cell lines (11–15), and also luminal cells of healthy breast tissue (14). From a zoological perspective, these data may not be entirely surprising since, e.g. in the common carp, small amounts of the globin were detected in various non-muscle tissues, including liver, gill, kidney and brain (25). The biological function of ectopic MB expression, however, has remained elusive up till now. In the present study, data mining of publicly available RNA-seq data sets have confirmed transcription of *MB* in several healthy and tumorous human tissues and cancer cell lines at mRNA levels corresponding to roughly 1/100 of the amount present in heart muscle (Fig. 2). Most importantly, detailed analyses of *MB* transcription revealed that the organization, splicing patterns and promoter usage of the *MB* gene are also much more complicated and variable than hitherto thought.

Unexpected complexity of the *MB* gene and its transcripts

Our EST and RNA-Seq data analyses revealed 11 alternative *MB* protein-coding transcripts in human tissues, the majority of which has been hitherto undescribed (Supplementary Material, Fig. S1).

An additional eight transcripts, producing aberrant or truncated MB versions, could be detected. However, their frameshift-induced premature stop codons in the *MB*-CDS are positioned distantly upstream of the distal 3′ splice site, making it likely that RNA-decay mechanisms (reviewed in: 26) degrade these transcripts prior to translation. This bewildering complexity of *MB* transcript variants is due to the presence of several novel exons within a substantially enlarged *MB* gene region of 31.8 kb instead of its former size of 16.6 kb. The *MB* gene thus illustrates results of the ENCODE project, stating that roughly 75% of the human genome is primarily transcribed (27). ENCODE cell lines were reported to express on average sets of 10–12 mRNA isoforms per gene, which agrees well with the expression of 9 and 6 alternative *MB* transcripts (out of 19 splice forms in total) in human skeletal and heart muscle, respectively. In cancer cell lines, 12 out of the 19 *MB* mRNA variants were detected (Supplementary Material, Fig. S1). Three of those variants, all hitherto undescribed, were most frequently observed in breast cancer entities, and one breast and one colon cancer cell line (Figs 3 and 4a). Thus, *MB* expression also adheres to the ENCODE rule that mostly one isoform per gene is predominantly expressed upon a certain cellular condition, and that 75% of all genes produce at least two major transcripts (27).

The obvious question for the adaptive functional value of multiple *MB* splice forms cannot be fully answered to date, but the observed transcriptional complexity is clearly contradictory to a ‘minimalistic expression strategy’ (27,28). As a possible example for the functionality of upstream exons, we found that the alternatively spliced cassette-exon 7 u is able to decrease *MB* translation efficiency via its part encoding a uORF (Fig. 6). Owing to the fact that the mRNA section between the uORF and the downstream *MB*-ORF is rather short (49 bp) and does not contain internal ribosome entry sites, we speculate that ribosome re-initiation is likely to be hindered to some extent when exon 7 u is spliced in (21,22,29,30). While the recorded effect on translation appears rather moderate *in vitro*, a non-linearity between MB protein and mRNA levels in a breast cancer cell line, possibly indicating post-transcriptional effects, has been reported previously (13). Notably, cassette-exon 7 u is part of an AluSc family element that was inserted into the *MB* gene, illustrating the potentially adaptive effect of retrotransposons as modulators of gene regulation during primate evolution (31–33). Various primate-associated transposons such as Alu and L1 elements have invaded the 5′ part of the human *MB* gene region (Supplementary Material, Fig. S3). Not surprisingly therefore, the novel *MB* upstream exons are only conserved throughout higher primate orders (Supplementary Material, Table S3) and lack orthologues in the mouse *Mb* gene, which displays less variability on the genomic level and in its splice patterns. Studying transcriptional regulation of ectopic *Mb* expression in the mouse may therefore be of limited value.

Most important to understand the gene regulatory mechanisms driving classic and ectopic *MB* expression is the fact that the alternative usage of 5′ upstream exons implies the existence of different promoters for the *MB* gene. For instance, *MB* transcript variants 2 and 5 are the most abundant mRNAs in heart and skeletal muscle (Fig. 2), but only variant 2 starts downstream of the classical TATA box motif (20). Interestingly, despite extensive work on this promoter region, which has led, e.g. to the identification of functionally relevant MEF2, Sp1 and NFAT transcription factor binding sites (34), the presence of an alternative transcriptional start site 5′ of starting exon 8 u has escaped notice so far, although it originates between the two NRE-elements and therefore covers the conventional promoter region. For the most active *MB* transcriptional start site in cancer cells, our reporter assays confirmed a 204 bp promoter section upstream of exon 5 u to confer high transcriptional activity in the *MB* expressing breast cancer cell line MDA-MB468. This section contains an integer CCAAT-box (also known as NF-Y), a motif that is often used to facilitate the transcription of genes over-represented in cancer (35). Further molecular studies are necessary to characterize the relevant gene regulatory elements of this tumor-associated *MB* promoter beyond mere bioinformatic predictions.

Cancer-associated human *MB* splice variants are hypoxia-regulated

The existence of additional promoter regions in the *MB* gene may clearly have the adaptive value of facilitating gene expression under special circumstances. From the viewpoint of tumor biology, it is an important finding that the *MB* transcripts initiated by the novel exon 5 u promoter (variants 9, 10, 11) are distinctly up-regulated by hypoxia, a frequent microenvironmental influence determining tumor physiology and malignancy (36,37; see discussion below). A 1.5–3.5 fold induction of those *MB* mRNAs was demonstrated *in vitro* in the breast cancer cell line MDA-MB468 and in DLD-1 colon cancer cells upon experimental hypoxia. In breast cancer biopsies, *MB* transcriptional up-regulation was paralleled by increased mRNA expression of the hypoxia-responsive *VEGFA* gene and on the protein level by positive immunostaining of the hypoxia-marker CAIX, suggesting that *MB* up-regulation at lowered oxygen levels also occurs *in vivo*. In line with these observations, we had previously reported (17) that another minor *MB* transcript (variant 13) also showed hypoxia-sensitivity (at 1% O_2) in MDA-MB468 breast cancer cells (but not in colon-derived DLD-1). Also, MB immunostaining distribution correlated with local tissue hypoxia in many cases of DCIS cancer entities, which originate in the breasts’ avascular milk ducts and completely rely on diffusional O_2 and nutrient supply, thus becoming more and more hypoxic towards their center during growth (17).

The degree of hypoxia-responsivity of the *MB* gene in the classic context of muscle cells has been a debated issue (38–42). Recent work showed that while the Mb content of the contracting heart of mice increased under moderate hypoxia (10% O_2), mouse Mb remained unchanged in sedated skeletal muscle (18). However, *MB* transcription in skeletal muscle could be induced by exercise via Ca^{2+} ion release to activate the calcineurin/NFAT pathway, with an increased calcineurin sensitivity upon hypoxia (18). Thus, at least in skeletal muscle, *MB* regulation does not respond to an isolated hypoxic stimulus, but requires a combination of exercise and hypoxia (reviewed in 34,43). In line with this finding, the muscle-associated standard *MB* promoter was reported to lack canonical binding sites for the hypoxia-responsive master transcription factors HIF-1α/-2α (19,18). In contrast, we have recently identified a candidate HRE within the upstream region of the *MB* gene that conferred a moderate 43% hypoxia induction to a downstream luciferase reporter gene (17). It is therefore probable that this HRE along with other, hitherto uncharacterized enhancer sites drives the

hypoxia-inducible transcription of *MB* mRNA variants in cancer cells. The recruitment of novel upstream exons and promoters in the primate lineage thus has facilitated evolution of an additional regulatory potential, which enables *MB* expression under hypoxic cellular stress. This potential appears to be specifically realized in a tumor context. It remains unclear, however, why a minor usage of the non-standard *MB* splice forms is also recorded in non-cancerous tissues, as observed in healthy breast, skeletal and heart muscle (comp. Fig. 2).

A non-standard molecular function of MB in hypoxic tumor tissues?

At current, the biochemical function of ectopically expressed MB in mammals is unclear. MB protein levels in breast tumor cells as well as in healthy breast tissue appear much too low to account for a respiratory function, suggesting a non-standard function of MB in tumor cells (17,44). This is even more likely, as work in myocytes has revealed important additional roles of MB, e.g. in compensating oxidative and nitrosative stress (7–10). In hypoxic tumor areas, an induction of (low-level) MB expression might interfere with the homeostasis between formation and sequestration of ROS and RNS (reactive nitrogen species), and subsequent biochemical studies will have to address these functional scenarios. Most importantly, MB-positive tumors reflect the luminal, better differentiated carcinoma phenotype along with an ameliorated prognosis for the patient, possibly due to advanced cell differentiation, less aggressiveness and reduced metastatic spread (13,14,16). Recent experiments on *MB* knockdown MDA-MB468 breast cancer cells indeed indicated that MB—by unknown mechanisms—impairs mitochondrial activity under hypoxia (17). MB therefore harbors the potential of acting as a tumor-suppressor, and its hypoxia-responsive up-regulation may partly explain its beneficial effect on breast tumor patients' survival.

MATERIALS AND METHODS

Bioinformatic analyses of the *MB* gene region

To elucidate the human and mouse *MB/Mb* gene structures, their corresponding EST files were downloaded from NCBI UniGene (http://www.ncbi.nlm.nih.gov/UniGene/clust.cgi?UGID=908333&TAXID=9606&SEARCH=mb, last accessed date on September 24, 2013) and aligned to the genomic *MB* sequence using the NCBI Spidey software (45). Novel exon regions and splice variants were portrayed with GenePalette 1.2 (46). All new splice variants were cross-checked with the transcripts available at NCBI AceView (http://www.ncbi.nlm.nih.gov/ieb/research/acembly/, last accessed date on September 24, 2013) and annotated, if a matching sequence has been found. We applied Gene2Promoter (www.genomatix.de, last accessed date on September 24, 2013) to predict the promoter sequences of novel 5′UTR splice variants (47). Common cis-acting promoter elements (TATA, CCAAT and GC boxes) were searched within the experimentally validated cancer-active *MB* promoter (Fig. 5) with ConSite (http://www.phylofoot.org/consite/, last accessed date on September 24, 2013), choosing a minimum specificity of 12 bits and a TF cut-off of 82%. All detected elements were then checked for the integrity of their essential core motif sites. The revised gene structures of human *MB* and mouse *Mb* were depicted with SeqBuilder (Lasergene Sequence Analysis Software, DNASTAR, Inc., USA). The positions of repeats relative to the newly identified exons were determined by RepeatMasker (http://www.repeatmasker.org, last accessed date on September 24, 2013) (48) and outlined on the human *MB* gene by SeqBuilder. All novel *MB* splice variants were inspected for encoded ORFs with EditSeq (Lasergene Sequence Analysis Software, DNASTAR, Inc., USA). Additionally, NCBI-BLASTX (49) searches were performed to reveal whether novel exons and exon combinations had protein coding potential. The phylogenetic conservation of newly found human *MB* exons was assessed in NCBI-BLASTN searches against the respective genes (plus a flanking 50 kb frame) of *Pan troglodytes* (2.1.4), *Macaca mulatta* (051 212), *Callithrix jacchus* (3.2), *Canis familiaris* (3.1), *Bos taurus* (UMD3.1), *Mus musculus* (GRCm38.p1), and *Gallus gallus* (4.0). Only hits with an e-value of $E < 1^{-10}$ were listed.

For an extended *de novo* detection of *MB* in different human tissues, high-throughput RNA-Seq data sets of different human tissues and cancer cell lines were downloaded from the NCBI Sequence Read Archive (SRA; see Supplementary Material, Table S4). All data sets were mapped against the genomic sequence of the *MB* gene (chromosome 22 of the human genome built 37) by applying the Tophat program package (http://tophat.cbcb.umd.edu/, last accessed date on September 24, 2013) with a maximum of two mismatches (default settings). To quantify *MB* exon usage in the different transcriptomes (Supplementary Material, Table S4) reads mapping to the coordinates of each *MB* transcript start exon (4 u, 5 u, 8 u, 9 u) and CDS-containing exons (9 c, 11 c and 12 c) were counted and normalized relative to the according exon and data set size to generate RPKM-values [reads per exon size (in kb) per 1 Mio. reads of the dataset]; (50). Dependent of the availability of tissue data sets on the SRA, average ratios were calculated via Excel 2003 (Microsoft) if multiple data sets per tissue type were used.

Characterization of *MB* splice variants in cancer cell lines

The breast cancer line MDA-MB468 and the colorectal adenocarcinoma cell line DLD-1 were cultured in DMEM/Hams-F12 with stable glutamine (PAA), supplemented with 10% FBS Gold (PAA) and 1% Pen/Strep (PAA). For normoxic culture conditions, cells were raised in an IG150 incubator (Jouan) at 5% CO_2 in an H_2O-saturated atmosphere at 37°C. For experimental hypoxia, cells were raised in a CB 53 incubator (Binder) in an H_2O-saturated atmosphere at 37°C, 1% O_2 and 5% CO_2.

To experimentally verify novel splice variants, total RNA was extracted from cell lines by applying the RNeasy Mini Kit (Qiagen), including a DNase I digestion. First-strand cDNA synthesis was carried out on 1 μg of total RNA using the Superscript III RT- Kit (Invitrogen). 5′/3′ RACE reactions were performed on RNA from MDA-MB468 cells using the Gene Racer Kit (Invitrogen). RT–PCRs on cDNA were conducted with the TrueStart Taq DNA Polymerase kit (Fermentas) in a peqSTAR 96 Universal Gradient Thermocycler (Peqlab) or T3 Thermocycler (Biometra), according to the manufacturer's instructions. Annealing temperatures were chosen in accordance with the melting temperatures of the primer sets. PCR amplicons were purified by the High Pure clean-up kit (Roche) and either sequenced directly or cloned into pGem-T Easy vectors (Promega). After transformation in DH10B-cells and

singularization of clones, plasmids were purified with the GeneJET Plasmid Miniprep Kit (Fermentas). Sanger-based sequencing reactions were carried out by a commercial service (StarSeq). Sequence reads of novel *MB* splice forms, such as *MB* sequences derived form 5′/3′ RACE reactions were submitted to the EMBL database (http://www.ebi.ac.uk/, last accessed date on September 24, 2013).

Quantitative real-time reverse-transcriptase PCR

The qRT–PCR reactions were performed on cDNA samples from hypoxic or normoxic MDA-MB468 and DLD-1 cells. The primer combinations used for each qRT–PCR reaction were chosen to specifically hybridize to only one *MB* splice variant of interest (see Fig. 3; Supplementary Material, Table S2). The Power SYBR Green PCR Mastermix (Applied Biosystems) was used at a total volume of 10 μl with annealing temperatures of 57°C in an ABI 7500 real-time cycler (Applied Biosystems).

For absolute quantification of samples with unknown cDNA content, we applied the standard curve approach with serial 10-fold dilutions of standard plasmids containing a matching amplicon as an insert. As a positive control for cellular response to hypoxic conditions, transcripts of the *VEGFA* gene were quantified in hypoxic and normoxic samples (51). Triplicate assays were measured in each run, with a total of $n = 3$ experiments for each amplicon assay. Average ratios and standard deviations were calculated via Excel 2003 (Microsoft). A two-sided Students' *t*-test with an error value of 5% ($\alpha = 0.05$) was performed to infer statistical significance.

Detection of *MB* splice variants in cancer biopsies

MB expression was analyzed in tumor and normal adjacent tissues obtained from surgical specimens from 21 primary breast cancer patients. Patient material was collected at the University Hospital of Bonn between 2007 and 2012. The study was approved by the institutional review board. Matched formalin-fixed and paraffin-embedded tissue (FFPET) and fresh-frozen tissues from the same patients were analyzed. MB and CAIX immunostaining of 3-μm FFPET sections was performed using the LabVision Autostainer 480S system (Thermo Scientific). The PT-Module was used for dewaxing and epitope retrieval (pH 6.0 at 99°C for 20 min). The following antibodies and dilutions were used: rabbit monoclonal MB antibody EP3081Y, (Abcam, Cambridge, UK), dilution 1:150; rabbit polyclonal CAIX antibody (Abcam), dilution 1:300.

Total RNA was isolated from the fresh-frozen tumor and normal adjacent tissues by means of the RNAeasy Kit (Qiagen), following the Animal Tissue protocol. As described above, the first-strand cDNA synthesis was conducted with the Superscript III RT- Kit (Invitrogen), but on 500 ng total RNA. The resulting cDNA was diluted 1:4 and quantified with the Qubit ssDNA Assay Kit (Life Technologies). qRT–PCRs were performed as described above, with the FastStart Universal SYBR Green Master (ROX) Mix (Roche) in duplicate assays. Absolute copy numbers of *MB* transcripts per 10 ng cDNA were determined using the standard curve approach. For statistical correlations, parametric Pearson tests were performed with SPSS, Version 21 (IBM SPSS Statistics). Samples were sorted according to the overall *MB* level detected in the biopsied tumors.

Functional analysis of a candidate uORF and a novel *MB* promoter via dual luciferase reporter assays

To investigate the functionality of the candidate uORF and the novel promoter, the corresponding sequence regions were amplified via PCR on human genomic placenta tissue DNA and cloned into luciferase reporter gene vectors (pGL3-control vectors, Promega). For PCR amplification of uORF and mutated uORF (c.-3067A > T) constructs, all forward and reverse primers were equipped with a 5′-end HindIII and NcoI site, respectively (Supplementary Material, Table S2). Forward and reverse primers used for the amplification of candidate promoter sections were engineered to carry 5′ MluI and HindIII recognition sites, respectively (Supplementary Material, Table S2). PCR reactions were prepared as described above. Annealing temperatures were in accordance with the melting temperatures of each primerset (see Supplementary Material, Table S2). Obtained PCR products were digested with the restriction enzymes that matched their flanking recognition sites. pGL3-control vectors (Promega) for cloning the uORF constructs and candidate promoter sections were digested with respective restriction enzymes (Fermentas). All vectors were then dephosphorylated at their 5′-ends by Antarctic Phosphatase (NEB). PCR products were ligated into the modified vectors using T4 ligase (Fermentas) and transformed as described above. We also generated a negative control vector lacking the SV40 promoter, by subjecting pGL3-control vector to a MluI/HindIII digest (Fermentas). After dephosphorylation and Klenow (NEB) end-filling of 5′ overhangs the blunt ended vector was ligated with T4 ligase (Fermentas) and transformed into bacterial host cells as described above.

About 10^4 MDA-MB468 cells were seeded in triplicates. By using 0.3 μl of the FuGENE-HD Transfection Reagent (Promega), all wells were co-transfected with 240 ng of pGL3-based firefly luciferase plasmids and 26 ng of pGL4.74 renilla luciferase vectors (Promega) as internal controls. After 44 h, DLRAs (Promega) assessed the influence of the uORF on the translation efficacies of the CDS and the transcriptional activity of different promoter constructs. Light signal intensity was quantified in a Glomax 96-well luminometer (Promega), choosing a sample volume of 40 μl for both luciferin reagents. Normalization of transfection efficacies was done by dividing the total amount of luciferase light units in each pGL3 sample by the co-transfected pGL4.74 renilla light units, yielding RLUs.

The RLU quantities of the mutated TTG (c.-3067A > T) uORF constructs were normalized on the RLU values of the ATG-uORF-constructs in each ($n = 5$) trial. RLU quantities of promoter constructs were normalized on RLUs of endfilled control vectors for enabling signal-to noise ratio estimation. For both, the uORF and the promoter experiments, standard deviations were calculated via Excel 2003 (Microsoft). A two-sided Student's *t*-test with an error rate of 1% ($\alpha = 0.01$) was performed to test for significance.

SEQUENCE ACCESSION NUMBERS

Accession numbers of sequence reads submitted to the EMBL database will be provided as soon as they are available.

SUPPLEMENTARY MATERIAL

Supplementary Material is available at *HMG* online.

ACKNOWLEDGEMENTS

We thank Carsten Golletz (UK Bonn) for expert technical assistance. This work was supported by the Center for Computational Sciences (SRFN) and a further intramural grant (Stufe 1) of Johannes Gutenberg University Mainz (to TH) and by the University Hospital Bonn (to GK).

Conflict of Interest statement. None declared.

REFERENCES

1. Kölliker, A. (1850) Mikroskopische Anatomie oder Gewebelehre des Menschen. *Verlag Wilhelm Engelmann Leipzig Germany*, **1**, 248.
2. Günther, H. (1921) Über den Muskelfarbstoff. *Virchows Archiv*, **230**, 146–178.
3. MacMunn, C.A. (1886) Researches on myohämatin and histohämatins. *J. Physiol.*, **5**, 24.
4. Wittenberg, B.A. and Wittenberg, J.B. (1989) Transport of oxygen in muscle. *Ann. Rev. Physiol.*, **51**, 857–878.
5. Wittenberg, J.B. and Wittenberg, B.A. (2003) Myoglobin function reassessed. *J. Exp. Biol.*, **206**, 2011–2020.
6. Wittenberg, J.B. (1970) Myoglobin-facilitated oxygen diffusion: role of myoglobin in oxygen entry into muscle. *Physiol. Rev.*, **50**, 559–636.
7. Flögel, U., Merx, M.W., Godecke, A., Decking, U.K. and Schrader, J. (2001) Myoglobin: a scavenger of bioactive NO. *Proc. Natl Acad. Sci. USA*, **98**, 735–740.
8. Flögel, U., Godecke, A., Klotz, L.O. and Schrader, J. (2004) Role of myoglobin in the antioxidant defense of the heart. *FASEB J.*, **18**, 1156–1158.
9. Shiva, S., Huang, Z., Grubina, R., Sun, J., Ringwood, L.A., MacArthur, P.H., Xu, X., Murphy, E., Darley-Usmar, V.M. and Gladwin, M.T. (2007) Deoxymyoglobin is a nitrite reductase that generates nitric oxide and regulates mitochondrial respiration. *Circ. Res.*, **100**, 654–661.
10. Helbo, S., Dewilde, S., Williams, D.R., Berghmans, H., Berenbrink, M., Cossins, A.R. and Fago, A. (2012) Functional differentiation of myoglobin isoforms in hypoxia-tolerant carp indicates tissue-specific protective roles. *Am. J. Physiol. Regul. Integr. Comp. Physiol.*, **302**, 693–701.
11. Ruck, P., Horny, H.P., Greschniok, A., Wehrmann, M. and Kaiserling, E. (1995) Nonspecific immunostaining of blast cells of acute leukemia by antibodies against nonhemopoietic antigens. *Hematol. Pathol.*, **9**, 49–56.
12. Zhang, P.J., Goldblum, J.R., Pawel, B.R., Fisher, C., Pasha, T.L. and Barr, F.G. (2003) Immunophenotype of desmoplastic small round cell tumors as detected in cases with EWS-WT1 gene fusion product. *Mod. Pathol.*, **16**, 229–235.
13. Flonta, S.E., Arena, S., Pisacane, A., Michieli, P. and Bardelli, A. (2009) Expression and functional regulation of myoglobin in epithelial cancers. *Am. J. Pathol.*, **175**, 201–206.
14. Kristiansen, G., Rose, M., Geisler, C., Fritzsche, F.R., Gerhardt, J., Lüke, C., Ladhoff, A.M., Knüchel, R., Dietel, M., Moch, H. *et al.* (2010) Endogenous myoglobin in human breast cancer is a hallmark of luminal cancer phenotype. *Br. J. Cancer*, **102**, 1736–1745.
15. Oleksiewicz, U., Daskoulidou, N., Liloglou, T., Tasopoulou, K., Bryan, J., Gosney, J.R., Field, J.K. and Xinarianos, G. (2011) Neuroglobin and myoglobin in non-small cell lung cancer: expression, regulation and prognosis. *Lung Cancer*, **74**, 411–418.
16. Galluzzo, M., Pennacchietti, S., Rosano, S., Comoglio, P.M. and Michieli, P. (2009) Prevention of hypoxia by myoglobin expression in human tumor cells promotes differentiation and inhibits metastasis. *J. Clin. Invest.*, **119**, 865–875.
17. Kristiansen, G., Hu, J., Wichmann, D., Stiehl, D.P., Rose, M., Gerhardt, J., Bohnert, A., ten Haaf, A., Moch, H., Raleigh, J. *et al.* (2011) Endogenous myoglobin in breast cancer is hypoxia-inducible by alternative transcription and functions to impair mitochondrial activity: a role in tumor suppression? *J.* Biol. Chem., **286**, 43417–43428.
18. Kanatous, S.B., Mammen, P.P., Rosenberg, P.B., Martin, C.M., White, M.D., Dimaio, J.M., Huang, G., Muallem, S. and Garry, D.J. (2009) Hypoxia reprograms calcium signaling and regulates myoglobin expression. *Am. J. Physiol. Cell Physiol.*, **296**, 393–402.
19. Wystub, S., Ebner, B., Fuchs, C., Weich, B., Burmester, T. and Hankeln, T. (2004) Interspecies comparison of neuroglobin, cytoglobin and myoglobin: sequence evolution and candidate regulatory elements. *Cytogenet. Genome Res.*, **105**, 65–78.
20. Weller, P., Jeffreys, A.J., Wilson, V. and Blanchetot, A. (1984) Organization of the human myoglobin gene. *EMBO J.*, **3**, 439–446.
21. Kozak, M. (1987) An analysis of 5′-noncoding sequences from 699 vertebrate messenger RNAs. *Nucleic Acids Res.*, **15**, 8125–8148.
22. Meijer, H.A. and Thomas, A.A. (2002) Control of eukaryotic protein synthesis by upstream open reading frames in the 5′-untranslated region of an mRNA. *Biochem. J.*, **367**, 1–11.
23. Hendgen-Cotta, U.B., Merx, M.W., Shiva, S., Schmitz, J., Becher, S., Klare, J.P., Steinhoff, H.J., Goedecke, A., Schrader, J., Gladwin, M.T. *et al.* (2008) Nitrite reductase activity of myoglobin regulates respiration and cellular viability in myocardial ischemiareperfusion injury. *Proc. Natl Acad. Sci. USA*, **105**, 10256–10261.
24. Qiu, Y., Sutton, L. and Riggs, A.F. (1998) Identification of myoglobin in human smooth muscle. *J. Biol. Chem.*, **273**, 23426–23432.
25. Fraser, J., de Mello, L.V., Ward, D., Rees, H.H., Williams, D.R., Fang, Y., Brass, A., Gracey, A.Y. and Cossins, A.R. (2006) Hypoxia-inducible myoglobin expression in nonmuscle tissues. *Proc. Natl Acad. Sci. USA*, **103**, 2977–2981.
26. Maquat, L.E. (2004) Nonsense-mediated mRNA decay: splicing, translation and mRNP dynamics. *Nat. Rev. Mol. Cell Biol.*, **5**, 89–99.
27. Djebali, S., Davis, C.A., Merkel, A., Dobin, A., Lassmann, T., Mortazavi, A., Tanzer, A., Lagarde, J., Lin, W., Schlesinger, F. *et al.* (2012) Landscape of transcription in human cells. *Nature*, **489**, 101–108.
28. Raser, J.M. and O'Shea, E.K. (2005) Noise in gene expression: origins, consequences, and control. *Science*, **309**, 2010–2013.
29. Kozak, M. (1999) Initiation of translation in prokaryotes and eukaryotes. *Gene*, **234**, 187–208.
30. Davuluri, R.V., Suzuki, Y., Sugano, S. and Zhang, M.Q. (2000) CART Classification of human 5′ UTR sequences. *Genome Res.*, **10**, 1807–1816.
31. Cordaux, R. and Batzer, M.A. (2009) The impact of retrotransposons on human genome evolution. *Nat. Rev. Genet.*, **10**, 691–703.
32. Shen, S., Lin, L., Cai, J.J., Jiang, P., Kenkel, E.J., Stroik, M.R., Sato, S., Davidson, B.L. and Xing, Y. (2011) Widespread establishment and regulatory impact of Alu exons in human genes. *Proc. Natl Acad. Sci. USA*, **108**, 2837–2842.
33. Cowley, M. and Oakey, R.J. (2013) Transposable elements re-wire and fine-tune the transcriptome. *PLoS Genet.*, **9**, e1003234.
34. Kanatous, S.B. and Mammen, P.P. (2010) Regulation of myoglobin expression. *J. Exp. Biol.*, **213**, 2741–2747.
35. Dolfini, D. and Mantovani, R. (2013) Targeting the Y/CCAAT box in cancer: YB-1 (YBX1) or NF-Y? *Cell Death Differ.*, **20**, 676–685.
36. Graeber, T.G., Osmanian, C., Jacks, T., Housman, D.E., Koch, C.J., Lowe, S.W. and Giaccia, A.J. (1996) Hypoxia-mediated selection of cells with diminished apoptotic potential in solid tumours. *Nature*, **379**, 88–91.
37. Michieli, P. (2009) Hypoxia, angiogenesis and cancer therapy: to breathe or not to breathe? *Cell Cycle*, **8**, 3291–3296.
38. Reynafarje, B. (1962) Myoglobin content and enzymatic activity of muscle and altitude adaptation. *J. Appl. Physiol.*, **17**, 301–305.
39. Hoppeler, H. and Vogt, M. (2001) Muscle tissue adaptations to hypoxia. *J. Exp. Biol.*, **204**, 3133–3139.
40. Masuda, K., Okazaki, K., Kuno, S., Asano, K., Shimojo, H. and Katsuta, S. (2001) Endurance training under 2500-m hypoxia does not increase myoglobin content in human skeletal muscle. *Eur. J. Appl. Physiol.*, **85**, 486–490.
41. Fordel, E., Geuens, E., Dewilde, S., De Coen, W. and Moens, L. (2004) Hypoxia/ischemia and the regulation of neuroglobin and cytoglobin expression. *IUBMB Life*, **56**, 681–687.
42. Gelfi, C., De Palma, S., Ripamonti, M., Eberini, I., Wait, R., Bajracharya, A., Marconi, C., Schneider, A., Hoppeler, H. and Cerretelli, P. (2004) New

aspects of altitude adaptation in Tibetans: a proteomic approach. *FASEB J.*, **18**, 612–614.
43. Wittenberg, B.A. (2009) Both hypoxia and work are required to enhance expression of myoglobin in skeletal muscle. Focus on Hypoxia Reprograms Calcium Signaling and Regulates Myoglobin Expression. *Am. J. Physiol. Cell Physiol.*, **296**, 390–392.
44. Gorr, T.A., Wichmann, D., Pilarsky, C., Theurillat, J.P., Fabrizius, A., Laufs, T., Bauer, T., Koslowski, M., Horn, S., Burmester, T. *et al.* (2011) Old proteins: new locations: myoglobin, haemoglobin, neuroglobin and cytoglobin in solid tumours and cancer cells. *Acta Physiol. (Oxf).*, **202**, 563–581.
45. Wheelan, S.J., Church, D.M. and Ostell, J.M. (2001) Spidey: a tool for mRNA-to-genomic alignments. *Genome Res.*, **11**, 1952–1957.
46. Rebeiz, M. and Posakony, J.W. (2004) Genepalette: a universal software tool for genome sequence visualization and analysis. *Dev. Biol.*, **271**, 431–438.
47. Scherf, M., Klingenhoff, A. and Werner, T. (2000) Highly specific localization of promoter regions in large genomic sequences by promoterInspector: a novel context analysis approach. *J. Mol. Biol.*, **297**, 599–606.
48. Saha, S., Bridges, S., Magbanua, Z.V. and Peterson, D.G. (2008) Empirical comparison of AB initio repeat finding programs. *Nucleic Acids Res.*, **36**, 2284–2294.
49. Altschul, S.F., Gish, W., Miller, W., Myers, E.W. and Lipman, D.J. (1990) Basic local alignment search tool. *J. Mol. Biol.*, **215**, 403–410.
50. Mortazavi, A., Williams, B.A., McCue, K., Schaeffer, L. and Wold, B. (2008) Mapping and quantifying mammalian transcriptomes by RNA-Seq. *Nat. Methods*, **5**, 621–628.
51. Hemmerlein, B., Galuschka, L., Putzer, N., Zischkau, S. and Heuser, M. (2004) Comparative analysis of COX-2, vascular endothelial growth factor and microvessel density in human renal cell carcinomas. *Histopathology*, **45**, 603–611.

SUPPLEMENTARY FIGURES

Table S1 (A). Table of representative Hsa *MB* EST accessions, supporting the respective splice variants. **Table S1 (B).** Table of representative Mmu *Mb* EST accession numbers and according splice variants.

Table S2. List of all primers applied. Restriction enzyme recognition sites are underlined.

Figure S1 (Top). Revised organization of the human *MB* gene. Untranslated exons (tagged with a 'u') are shown in blue color while CDS-encoding exons (tagged with a 'c') are red. Annotation of the *MB*-CDS start and stop codons are included. (Below). Presence of *MB* splice variants in different tissues. For each tissue, the number of representing ESTs is indicated. Green: *MB* transcripts detected in MDA-MB468 and DLD-1 via qRT-PCR. Hashes indicate transcripts whose integrity has been approved by 5'-RACE reactions. On the right hand side of the splice variants, the corresponding NCBI-AceView annotation letters are written in parentheses and protein encoding splice variants are marked with a Y. The standard MB gene promoter of variant 2 and the additional five predicted promoter regions are indicated.

Table S3. Conservation between human *MB* exons and the corresponding gene sequences (flanked by a 50kb frame) of other species. Displayed are hits with an e-value (E<1^-10) and their percent nucleotide identities. Yellow: CDS-containing exons.

Figure S2 (A). Comparison of the Hsa *MB* and Mmu *Mb* gene structures. **Figure S2 (B).** (Top): Revised organization of the mouse *Mb* gene, exon-intron structure. The size of each exon is written on its top. Untranslated exons (tagged with a 'u') are shown in blue color

while CDS-encoding exons (tagged with a ‘c’) are red. Annotation of the *Mb*-CDS start and stop codons are included. (Below): Presence of mouse *Mb* splice variants in different tissues (the corresponding number of ESTs are indicated). On the right hand side of the splice variants, the according NCBI-AceView annotation letters are written in parentheses and protein encoding splice variants are marked with a Y. Predicted promomoter regions are indicated as green boxes.

Figure S3. Repetitive elements in the human *MB* gene region. Exon positions are highlighted in blue and red. Repeats are marked as arrows, according to their class and orientation.

Table S4. Datasets analyzed from the NCBI-Sequence Read Archive (SRA). Originating tissues are listed on the left.

Table S1 (A). Table of representative Hsa *MB* EST accessions, supporting the respective splice variants.

Acc.No	Tissue	Dev. stage	Variant	Exon 1u	Exon 2u	Exon 3u	Exon 4u	Exon 5u	Exon 6u	Exon 7u	Exon 8u	Exon 9u	Exon 9c	Exon 10u	Exon 11c	Exon 12c
exon size				**218 bp**	**86 bp**	**103 bp**	**164 bp**	**113 bp**	**132bp**	**116 bp**	**225 bp**	**72 bp**	**103 bp**	**140 bp**	**223 bp**	**679 bp**
2938944	skeletal muscle		1											140	x	
21806536	coronary artery endothelial cells		2									x	x		x	x
21828777	heart		2									66	x		x	x
21829059	heart		2									64	x		x	x
21887456	muscle		2									64	x		x	x
21887573	muscle		2									68	x		x	x
4711867	sciatic nerve		2									51	x		x	x
29149305	skeletal muscle		3									64	x +86bp		x	x
20993663	heart		4									x	x		till 104	from 373
21826735	heart		5								75		x		x	x
21827048	heart		5								71		x		x	x
16843686	liver	fetal	5								71		x		x	x
2800052	prostate		5								71		x		x	x
566930	skeletal muscle		5								63		x		x	x
1490850	prostate		6								5		x		till 79	from 327
29129213	skeletal muscle		7								31+ Intron	x	x		x	x
29217103	skeletal muscle		7								71+ Intron	x	x		x	x
29172333	skeletal muscle		8								147+79		x		x	x
4742007	large cell carcinoma cell line (lung)		9					29					x		x	x
21776299	muscle	fetal	9					84					x		x	x
29148116	skeletal muscle		9					79					x		x	x
709887	total fetus	8-9weeks	12					31							x	x
3045051	adrenal cortex carcinoma cell line		13				164						x		x	x
4150768	ascites cancer cell line		13				129						x		x	x
29126033	skeletal muscle		14				116			116					x	x
599575	heart	8-10weeks	15			153									x	x
4656873	adenocarcinoma cell line		16				48+164						x		x	x
	testis2		18		93	103							x		x	x

Table S1 (B). Table of representative Mmu *Mb* EST accession numbers and according splice variants.

Acc.No	Tissue	Dev. stage	Variant	Exon 1u	Exon 2u	Exon 3u	Exon short4u	Exon 4u	Exon 4c	Exon 5u	Exon 6c	Exon 7c
exon size				**143 bp**	**85 bp**	**74 bp**	**65 bp**	**203 bp**	**105 bp**	**77 bp**	**224 bp**	**588 bp**
9943731	heart		1							77	x	x
7851096	diaphragm		2					194	x		x	x
26679870	eye		2					49	x		x	x
10023174	heart		2					48	x		x	x
21709940	muscle		2					5	x		x	x
7374498	diaphragm		3				34		x		x	x
10022213	heart		3				54		x		x	x
7270694	liver		3				54		x		x	x
8951593	salivary gland		3				51		x		x	x
9171407	skeletal muscle		4					41	x		till 63	from 338
10779292	brain		5			74			x		x	
9442696	heart		6	167					x		x	x
8764040	mammary gland tumor		6	133					x		x	x
9771898	tumor gross tissue		7	45	85				x		x	x

Table S2. List of all primers applied

Name		Sequence (5' --- 3')	Application
Ex1	for	ACATTCCCAGAGAGTCTTGG	RT-PCR
Ex2	for	GAAGCCTCCTGTTGGGTAG	
Ex3	for	GCACCTGAGTTCCAAAGGAG	
Ex5	for	AGGACAGCTGGGGAGAAG	
Ex8	for	GCATGTTGGCCTGGTCCTTTGC	
Ex10	for	GGTTGAGCGAAGGGATTGTC	
Ex9ctag	for	CCACCCACACCCTAAGATCA	
Ex3	rev	CATCCCAGCTCCATCTCAAG	
Ex9	rev	CCCAGACGTTCAGCACCAACTGCC	
Ex12	rev	CATGCAGAACACAGTGAGCC	
Ex3	rev	CATCCCAGCTCCATCTCAAG	5'RACE
Ex4	rev	CTCACTCTCTCACCTGCTC	
Ex5	rev	AGCTGTCCTCGCAGAGCCT	
Ex1/3	for	CACCTGTGAATGCTTGAATTGC	3'RACE
Ex4a	for	GCTAGGTACTGTAGAGCAGG	qRT-PCR on MB468 and DLD-1
Ex4b	for	GCATGTTGGCCTGGTCCTTTGC	qRT-PCR on Matched Samples
Ex9u	for	CCCAGTGAGCCCATACTTGC	qRT-PCR on MB468, DLD-1 and Matched Samples
Ex9/11	rev	CTTAAAGAGCCTGATGAGGAC	
Ex5/9	for	GAGCTGTGACTGCGCCATG	
Ex6/9	for	TGTGCAGACTGCGCCATG	
Ex7/9	for	GACTACAGACTGCGCCATG	
Ex11	rev	GCCTTCATCTCGTCCTCTGAC	
VEGFA	for	AGGAGGAGGGCAGAATCATCA	
VEGFA	rev	CTCGATTGGATGGCAGTAGCT	
uORF-ATG	for	NNNNAAGCTTGGGGAGCTGTATGGAGGCTCG	uORF with *HindIII* (for) and *NcoI* (rev) sites (underlined)
uORF-TTG	for	NNNNAAGCTTGGGGAGCTGTTTGGAGGCTCG	
uORF	rev	NNNNCCATGGCGCAGTCTGTAGTCCCAGCTA	
+501	for	NNNNACGCGTTGTCCCTGGTGTGCACTAAG	Promoter upstream to exon 5u with *MluI* (for) and *HindIII* (rev) sites (underlined)
+335	for	NNNNACGCGTCACATCTGCTGGGAATGGGTAG	
+224	for	NNNNACGCGTACTGTGGAGGCGGGGCTGGTC	
+179	for	NNNNACGCGTTGGAGCTGGAGGAGCCACTC	
+108	for	NNNNACGCGTGGCCACACCTGTTGACTAAGG	
-17	rev	NNNNAAGCTTCACAGGGAACTAAAAATACAGTT	
-25	rev	NNNNAAGCTTGGGAGAGGCACAGGGAACTAA	
-191	rev	NNNNAAGCTTCAAGCTTGCTCCAGACTCCC	

Figure S1. Revised organization of the human *MB* gene

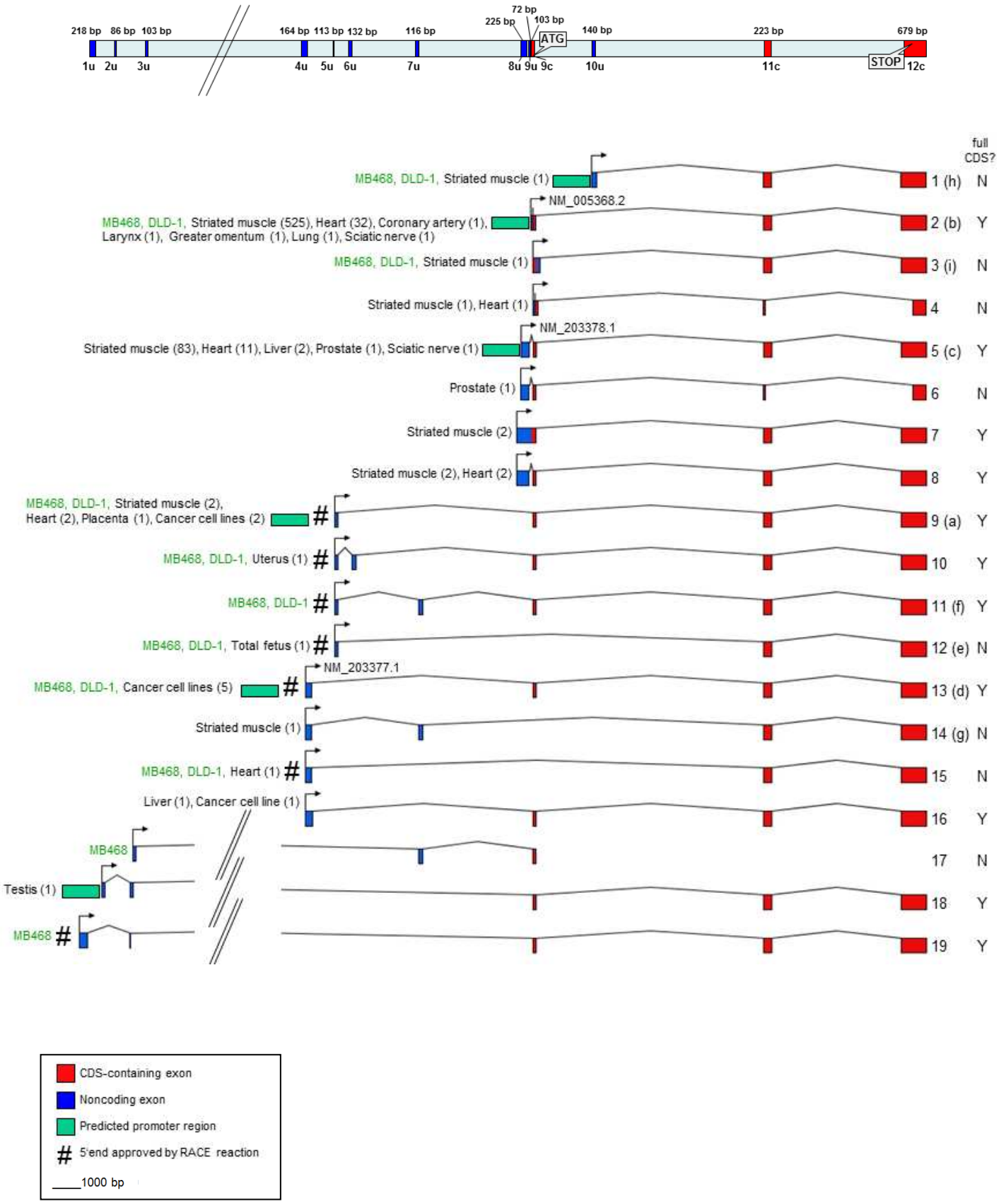

Table S3. Conservation between human *MB* exons and the corresponding gene sequences (flanked by a 50kb frame) of other species

Exon	Chimpanzee	Macaque	Marmoset	Dog	Cattle	Mouse	Chicken
1u (218 bp)	5e-105; Identities: 213/218(98%)	2e-86; Identities: 199/218(91%)	--	3e-19; Identities: 117/155(75%)	--	--	--
2u (86 bp)	3e-39; Identities: 85/86(99%)	4e-38; Identities: 83/85(98%)	--	--	--	--	--
3u (103 bp)	5e-50; Identities: 103/103(100%)	7e-43; Identities: 100/107(93%)	--	--	--	--	--
4u (164 bp)	3e-80; Identities: 162/164(99%)	5e-58; Identities: 126/132(95%)	5e-64; Identities: 150/164(91%)	--	--	--	--
5u (113 bp)	2e-55; Identities: 113/113(100%)	2e-54; Identities: 112/113(99%)	3e-46; Identities: 108/115(94%)	6e-37; Identities: 98/109(90%)	1e-33; Identities: 94/108(87%)	--	--
6u (132 bp)	6e-63; Identities: 130/132(98%)	1e-63; Identities: 130/132(98%)	9e-47; Identities: 119/132(90%)	--	--	--	--
7u (116 bp)	6e-50; Identities: 114/121(94%)*	1e-31; Identities: 97/115(84%)*	3e-33; Identities: 101/119(85%)*	--	--	--	--
8u (225 bp)	2e-109; Identities: 221/225(98%)	3e-106; Identities: 217/224(97%)	9e-88; Identities: 211/237(89%)	1e-42; Identities: 172/220(78%)	8e-39; Identities: 130/158(82%)	3e-27; Identities: 89/104(86%)	--
9u (72 bp)	2e-33; Identities: 72/72(100%)	1e-28; Identities: 65/67(97%)	4e-29; Identities: 69/72(96%)	3e-18; Identities: 58/67(87%)	8e-20; Identities: 62/72(86%)	--	--
9c (103 bp)	5e-50; Identities: 103/103(100%)	6e-48; Identities: 101/103(98%)	8e-46; Identities: 100/103(97%)	5e-37; Identities: 90/97(93%)	7e-42; Identities: 97/103(94%)	2e-30; Identities: 84/95(88%)	2e-15; Identities: 74/97(76%)
10u (140 bp)	2e-63; Identities: 134/138(97%)	2e-49; Identities: 124/138(90%)	9e-35; Identities: 113/138(82%)	3e-10; Identities: 68/93(73%)	1e-20; Identities: 92/119(77%)	--	--
11c (223 bp)	2e-109; Identities: 219/223(98%)	3e-100; Identities: 212/223(95%)	1e-85; Identities: 201/222(91%)	1e-80; Identities: 198/223(89%)	1e-68; Identities: 189/223(85%)	3e-65; Identities: 186/222(84%)	1e-35; Identities: 157/210(75%)
12c (679 bp)	9e-127; Identities: 249/251(99%); 2e-167; Identities: 326/329(99%)	0.0; Identities: 630/683(92%)	0.0; Identities: 576/683(84%)	3e-82; Identities: 504/725(70%)	3e-63; Identities: 337/467(72%)	1e-36; Identities: 147/189(78%)	2e-26; Identities: 115/148(78%)

* More than one sufficient (<1^-10) hit

Figure S2 (A). Comparison of the Hsa *MB* and Mmu *Mb* gene structures

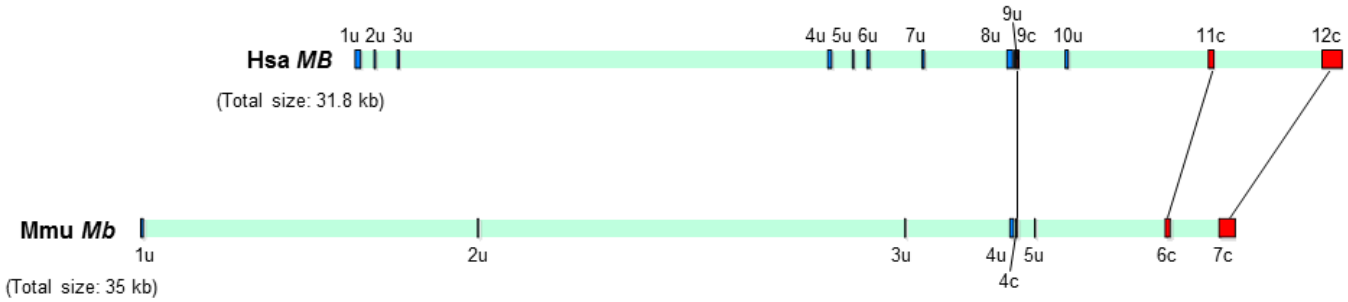

Figure S2 (B). Revised organization of the mouse *Mb* gene

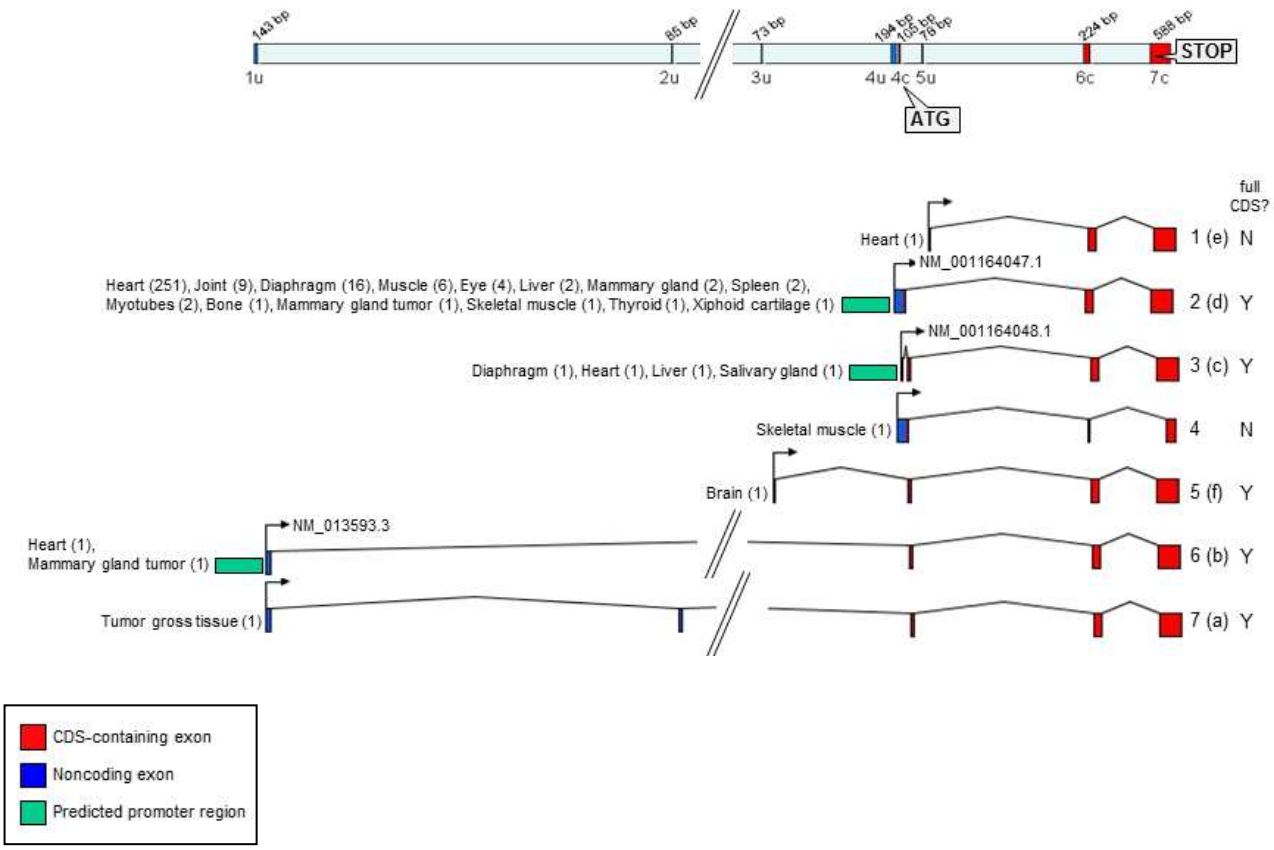

Figure S3. Repetitive elements of the human *MB* gene

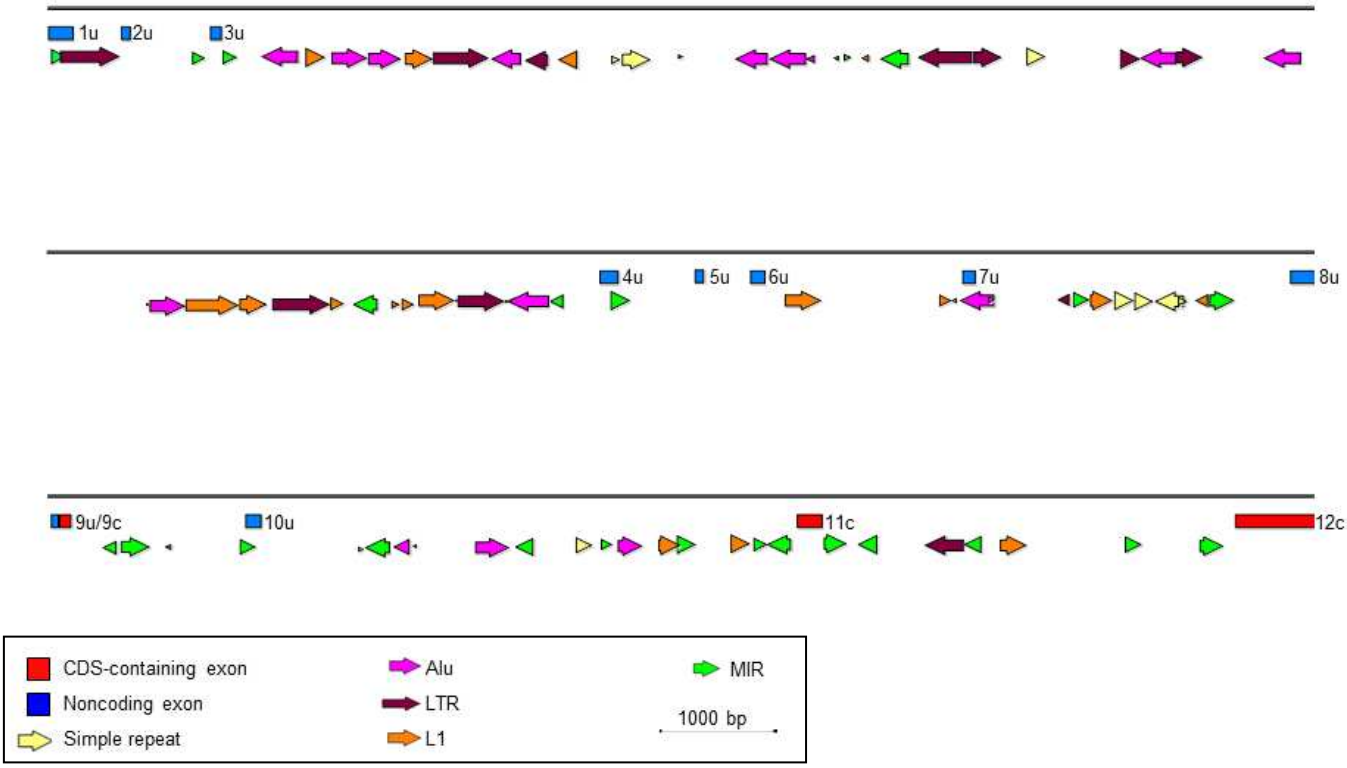

Table S4. Datasets analyzed from the NCBI-Sequence Read Archive (SRA)

Heart	SRR015300	SRR015301	SRR015303	SRR015304	SRR015305	SRR015306	
Muscle	SRR015307	SRR015308	SRR015309	SRR015311	SRR015312	SRR015313	
Breast	SRR015270	SRR015271	SRR015272	SRR015273			
Colon	SRR015314	SRR015315	SRR015316	SRR015317	SRR015318	SRR015319	SRR015320
LNCaP	SRR202054	SRR202058	SRR202059	SRR202060			
MCF7	SRR015274	SRR015275	SRR015276	SRR015277	SRR097789		
MDA-MB468	SRR097791						
DLD-1	DRR000014	DRR000015	DRR000016				
Prostate cancer	SRR057630	SRR057643	SRR057646				
Colon cancer	SRR222176	SRR222178					